ZnO Materials as Effective Anodes for the Photoelectrochemical Regeneration of Enzymatically Active NAD+

Publisher copyright

(Article begins on next page)

12 May 2024

ZnO materials as effective anodes for the photoelectrochemical regeneration of enzymatically active NAD^{+}

Carminna Ottone [a]*, Diego Pugliese [b], Marco Laurenti [b], Simelys Hernández [b], Valentina Cauda [b], Paula Grez [c], Lorena Wilson [a]

[a] Escuela de Ingeniería Bioquímica, Pontificia Universidad Católica de Valparaíso, Av. Brasil 2085, Valparaiso, Chile

[b] Department of Applied Science and Technology, Politecnico di Torino, C.so Duca degli Abruzzi 24, 10129, Turin, Italy.

[c] Instituto de Química, Pontificia Universidad Católica de Valparaíso, Av. Universidad 330, Curauma, Chile

KEYWORDS

ABSTRACT

This work reports the study of ZnO-based anodes for the photoelectrochemical regeneration of the oxidized form of nicotinamide adenine dinucleotide (NAD$^+$). The latter is the most important coenzyme in nature, where dehydrogenases use it in redox reactions. However, the high costs of NAD$^+$ limit the use of such enzymes at the industrial level. The ZnO films were prepared by three different routes, namely hydrothermal method, tape-casting, and sputtering. The detection of diluted solutions (0.1 mM) of the reduced form of the coenzyme (NADH) was accomplished by the flower-like and the porous films, whereas concentrations greater than 20 mM were needed for the detection of NADH with nanowire-shaped ZnO-based electrodes. The photocatalytic activity of ZnO was reduced at increasing concentrations of NAD$^+$ because part of the UV irradiation was absorbed by the coenzyme, reducing the photons available for the ZnO material. The higher electrochemical surface area of the flower-like film makes it suitable for the regeneration reaction. The illumination of the electrodes led to a significant increase on the NAD$^+$ regeneration with respect to both the electrochemical oxidation in dark and the only photochemical reaction. The tests with formate dehydrogenase demonstrated that 94% of the regenerated NAD$^+$ was enzymatically active.

1. Introduction

Enzyme technology is part of the biotechnology discipline that has shown systematic growth in the last years since it results to be a sustainable alternative to traditional chemistry processes. In particular, oxidoreductases have been investigated for redox processes [1-5]. A large number of oxidoreductases (>300) is dependent of expensive redox coenzymes, which need to be regenerated to proceed with the reaction [6]. In natural oxidation systems, dehydrogenases use the oxidized form of nicotinamide adenine dinucleotide, NAD^+, which is reduced to NADH. Two electrons and one proton are involved in the conversion reaction between the reduced and oxidized NAD species [7]. In living cells, NADH is oxidized back to the NAD^+ form by means of other enzymatic reactions taking part in the cell.

The high cost of the coenzymes is the main limitation which prevents the use of dehydrogenases at the industrial level [8]. Therefore, the design of an efficient, simple, low-cost and in situ coenzyme regeneration system is necessary [9]. Enzymatic [10-11], chemical [12], electrochemical [5-6, 13-15], photochemical [16] or photoelectrochemical [17-18] approaches have been proposed. Among the enzymatic approaches, NADH oxidase [19], formate dehydrogenase [20] and phosphite dehydrogenase [21] are the most studied ones. However, coupling the enzyme to a second enzymatic reaction is expensive, unstable and makes the product isolation more difficult. The electrochemical method uses the electric current to supply the energy required for the redox reaction of the coenzyme on the surface of the electrodes. The main drawback of this technology with respect to the enzymatic approach is the low turnover number [13]. Nonetheless, the electrochemical regeneration of the coenzyme gives a cost effective technology that is easy to monitor.

The redox couple $NAD^+/NADH$ has a reduction potential of -0.32 V *vs*. standard hydrogen electrode (SHE) [22]. Both direct and mediated approaches have been studied. The use of dissolved mediators in the media has proven to reduce the overpotential [7, 23]. However, the most used redox mediators, such as metal complexes [24], quinones [25], o-, p-phenylenediimines [26] and metal ions [27], or their precursors, are water contaminants with carcinogenic and /or mutagenic effect in nature [28]. The use of a direct electron transfer highlights several advantages: no co-substrate is required and no side-products are formed, no second enzyme is needed and the technique is environmentally friendly [29]. However, direct anodic oxidation of NADH usually lead to enzymatically inactive products [30-31]. The highest conversions of NADH to active NAD^+ were achieved by using noble metal-based anodes (e.g. gold and platinum) [32], which make the direct electrochemical regeneration a process not economically feasible. Therefore, considerable efforts are focused towards finding new anode materials based on earth abundant elements.

ZnO is a member of the II-VI group of semiconductors, with a band gap (E_g) of ~3.3 eV [33-34]. Nanostructured ZnO was extensively employed as photocatalyst for water oxidation reaction [34], dyes degradation [35] or for solar cells [36]. The advantages of using nanostructured ZnO-based electrodes rely on their unique advantages; high specific surface area, no toxicity, chemical stability and electrochemically-active properties. Besides, ZnO can be synthesized with different shapes [37-38] by various methods, including sol-gel [33], hydrothermal [39], electrodeposition [40], and physical deposition [41], among others. Modified ZnO electrodes have been studied for enzymatic biosensing applications [42], in the detection of L-lactic [43], urea [44], glucose [45], among others, due to the ability of this

material to oxidize NADH. The proper enzyme, that can be dissolved in the media or immobilized on a support, recognizes the analyte of interest as its substrate and oxidizes it with the formation of a stoichiometric amount of NADH. The latter is then recognized by the ZnO-based sensor. However, the effect of illumination on the semiconductor was hardly studied and only few works using TiO_2 are found in literature [17]. To the best of our knowledge, no studies of the photocatalytic effect on the electrochemical regeneration of NAD^+ with ZnO-based electrodes are reported. The similar photocatalytic properties between TiO_2 and ZnO, in terms of band gap, electronic levels, and good electron mobility, make the latter an interesting material to be studied in the photoelectrochemical regeneration of NAD^+.

The aim of this work is to study three different ZnO nanostructures as anodes for the photoelectrochemical regeneration of NAD^+. The anodes were prepared by three routes: i) hydrothermal method, which yields to the formation of nanowire-shaped ZnO crystals; ii) tape-casting of a previously synthesized ZnO powder with a flower-like shape; and iii) deposition of Zn films by radio-frequency magnetron sputtering then processed by thermal oxidation, yielding to the formation of a porous ZnO film.

NAD^+-dependent formate dehydrogenase was studied as a model enzyme to evaluate the enzymatic activity of the regenerated coenzyme.

2. Experimental Section

2.1 Materials

Zn(NO$_3$)$_2$·6H$_2$O, Zn acetate, polyethyleneimine (PEI, M = 800 g·mol^{-1}, end capped),

Na$_2$SO$_4$, NaH$_2$PO$_4$·2H$_2$O, Na$_2$HPO$_4$·H$_2$O and hexamethylenetetramine (HMT) were

purchased from Sigma-Aldrich and potassium hydroxide (KOH) from Merck. The

nicotinamide based coenzymes, NAD$^+$ and NADH, were purchased from GERBU GmbH,

the Fluorine-doped Tin Oxide (FTO) covered glasses from Solaronix, and the formate

dehydrogenase from *Candida boidinii* (Creative Enzymes).

2.2 Synthesis of ZnO nanowires (ZnOW)

The ZnO nanowire films (ZnOW) were synthesized through the aqueous chemical growth

approach [46]. First, a ZnO seed layer was deposited on a FTO slide by dip-coating the

substrate in a 5 mM zinc acetate solution in ethanol. The FTO slide was heated up to 300 ºC

for 10 min. Then, the FTO slide was immersed in a solution containing 50 mM zinc nitrate

hexahydrate (Zn(NO$_3$)$_2$·6H$_2$O), 25 mM hexamethylenetetramine (HMT), 1.5 mM

polyethyleneimine (PEI) and 320 mM ammonium hydroxide in bi-distilled water and

maintained at 88 ºC for 3 h under stirring.

2.3 Synthesis of porous ZnO based films (ZnOP)

The porous zinc oxide thin films (ZnOP) were prepared on FTO-coated glass substrates

according to a two-step synthetic approach [47]. In short, the preparation process consisted

of the deposition of metallic and porous zinc (Zn) films by radio-frequency (RF) magnetron

sputtering (step 1), followed by a thermal oxidation process (step 2) to get the conversion of

the metallic films into ZnO. The sputtering process was carried out starting from a 4-inch

diameter metallic Zn target, in pure Ar atmosphere. A RF voltage (working frequency 13.56

MHz, power density 0.66 W·cm^{-2}) was applied to the cathode on which the target is clamped,

and used to create the plasma. The target-to-substrate distance was about 8 cm. Suitable high-vacuum conditions were obtained with a rotary and a turbo molecular pump. The Zn deposition was performed at a fixed Ar gas pressure of $5 \cdot 10^{-3}$ Torr and without providing any intentional heating to the substrates. The overall deposition time was set to 2 h. Before starting the deposition process, the target was cleaned with a 15 min sputtering process to avoid any incorporation of contaminants in the Zn films. Finally, the porous Zn films were oxidized in a muffle furnace, operating at 380 °C in ambient air for 2 h.

2.4 Synthesis of ZnO flowerlike-based films (ZnOF)

The ZnO flowerlike microparticles (ZnOF) were synthesized by a hydrothermal method reported in detail elsewhere [48]. Briefly, 2.8 g of potassium hydroxide (KOH, 1 M) and 7.4 g of zinc nitrate hexahydrate ($ZnNO_3 \cdot 6H_2O$, 0.5 M) were dissolved separately in 50 mL of bi-distilled water (from Direct-Q system, Millipore). The zinc nitrate aqueous solution was then mixed drop by drop into the KOH precursor under vigorous stirring, thus obtaining a white gel. The gel was transferred in a closed autoclave with Teflon lining and kept at 70 °C for 4 h. The ZnO microparticles were filtered and washed with deionized water until neutral pH and dried overnight at 60 °C in ambient atmosphere.

The as-grown ZnO flowerlike particles were dispersed in a solution containing acetic acid, ethanol and water [36] and then sonicated for 4 h in order to obtain a homogeneous paste. Subsequently, a circular shaped ZnO layer was deposited onto preliminary cleaned FTO covered glasses by means of the tape-casting technique. The films were dried at 90 °C for 30 min and thermally treated at 450 °C for 10 min in air. The final thickness of the ZnO films was measured by using a profilometer (P.10 KLA-Tencor Profiler).

2.5 Physicochemical characterization of the ZnO-based films

The morphology of the ZnO nanostructures was investigated by means of the Field Emission Scanning Electron Microscopy (FE-SEM, Dual Beam Auriga from Carl Zeiss, operating at 5 keV). The X-Ray Diffraction (XRD) technique was performed to evaluate the crystalline structure of the produced ZnO anodes (X′Pert diffractometer, Cu K_α = 1.54 Å). IR spectra were acquired in Attenuated Total Reflectance mode with 2 cm^{-1} resolution and 64 scans accumulation, using a Nicolet 5700 FTIR Spectrometer (ThermoFisher, Waltham, MA, USA). Each spectrum is background subtracted. UV-Visible (UV-Vis) reflectance spectra F(R) were collected with a spectrophotometer (Varian Cary 500) by using an integrating sphere. Band-gap was calculated from the UV-Vis spectra as reported elsewhere [34]. For more information, see the Supplementary Information (SI).

2.6 Photoelectrochemical characterization of the films

Photoelectrochemical measurements were performed with a three-electrode glass cell with a quartz window. The reference electrode was Ag/AgCl (3 M KCl) and a Pt wire served as counter electrode. The data recording was performed with a multichannel VSP potentiostat/galvanostat (BioLogic), equipped with EC-Lab v. 10.1x software. The catalytic activity of ZnO films towards NADH oxidation was tested at pH = 7.0 in 100 mM sodium phosphate buffer. The solution was degassed for 30 min with N_2 before each experiment. All applied potentials are given *vs*. Ag/AgCl. Cyclic voltammetries (CVs) and linear sweep voltammetries (LSVs) were performed in the range between 0 and 1.6 V with a sweep rate of 20 mV·s^{-1}. The NADH concentration varied from 0 to 20 mM, as indicated. Current density (j) was calculated by considering the electrochemical surface area (ECSA) of the ZnO nanostructured films (see SI). LSV curves were acquired in the dark and under chopped light irradiation. The intensity of the light was maintained at 180 mW·cm^{-2} (39.7 mW·cm^{-2}

in the UV range: 280 to 400 nm) by adjusting the distance between the light source (i.e. Newport 450 W Xe lamp equipped with an AM 1.5G filter and a water filter model 6123NS) and the photoelectrochemical cell (PEC). Tafel plots were obtained from the oxidation peak extracted from the LSVs performed in the range between 0.4 and 1.6 V and using a scan rate equal to 1, 2, 5, 10, 20 and 100 mV·s^{-1} with 1 mM NADH solution. The potential was corrected with the ohmic resistance of the solution ($R_S \sim 40$ Ω) measured at each potential/current step at 10 kHz and 20 mV of modulation amplitude.

2.7 Regeneration of NAD$^+$

Chrono-amperometry (CA) measurements were performed in the presence of 1 mM NADH at the open circuit voltage (OCV) and 1.2 V *vs*. Ag/AgCl under dark conditions and under illumination, as indicated. The oxidation of NADH, Eq. 1, was monitored spectrophotometrically by the solution absorbance decrease at 340 nm for 3 h.

$$NADH \rightarrow NAD^+ + H^+ + 2\,e^- \quad (1)$$
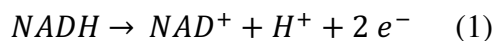
The activity of regenerated NAD$^+$ was determined spectrophotometrically by using formate dehydrogenase (FDH) enzyme for the oxidation of the formate species as described in Eq. 2.

$$Formate + NAD^+ \xrightleftharpoons{FDH} CO_2 + NADH + H^+ \quad (2)$$
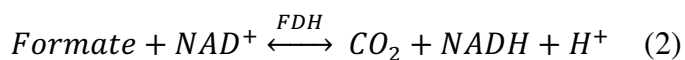
Briefly, 100 μL of FDH sample was added to the spectrophotometer cell with 2.8 mL sodium formate solution (final concentration 58 mM) and 100 μL of oxidized 1 mM NADH solution. The reaction solution was buffered to pH 7.5 with 100 mM sodium phosphate. The enzymatic solution was incubated at 30 ºC for 1 min and the formation of NADH was

measured at 340 nm. The relative enzymatic activity of the regenerated NADH solution was determined by using a fresh NAD$^+$ solution (1 mM) as reference.

3. Results and discussion

3.1 Morphological and structural characterization of ZnO nanostructures and films

Figure 1 shows the FE-SEM images of the prepared ZnO anodes. The crystals of ZnOW have grown up perpendicular to the FTO surface as shown in Figure 1a. The base of the wires showed a thickness of ~170 nm, becoming thinner towards the tip. The flowerlike aggregates of ~2 μm in diameter showed nanosized multipetals found in the starting powder form, as reported previously [49]. This peculiar morphology is preserved after the manufacture of the photoanode (Figure 1b). Only a little smoothing of the sharp edges was observed possibly due to the slight dissolution effect induced by the acetic acid-based solution. The morphology of the ZnOP film is shown in Figure 1c. The film is made of nanoparticles that are interconnected between them, resulting into a 3D matrix with porosities of irregular shape and different dimensions [47].

The XRD patterns of the three ZnO structures (Figure 2a) show the diffraction peaks of a pure hexagonal wurtzite structure (JCPDS file, No. 80-0074). The samples ZnOW and ZnOF showed sharp peaks that pointed out a good crystalline quality. The highest intensity at 34° of the ZnOW indicates a preferred growth of the crystals along the [001] direction. As for ZnOF and ZnOP, all peaks display similar intensities, which indicates that the ZnO crystals have no specific orientation growth.

The ZnO films absorbed in the UV region, as confirmed from the UV-Vis spectra shown in Figure 2b. The band gap of each ZnO film morphology, reported in Table 1, was calculated

from the UV-Vis spectra. ZnOF showed the smallest band gap, followed by ZnOW and ZnOP. The values are in line with those reported in literature [33].

3.2. Electrochemical oxidation of NADH

The electrochemical tests were performed by covering the films with a mask having a circular-shaped opening of 1.0 cm in diameter. The geometrical area (GA) of the active ZnO materials was equal to 0.78 cm^2 for all cases. The electrochemical surface area (ECSA) was calculated taking into consideration the effective active area (see the S.I. for more details), which varies among the ZnO anodes because of their different structure and thickness. The values are reported in Table 1. ZnOF showed an ECSA value 4-fold higher than the other two films. Such a pronounced value is mainly attributed to its higher thickness. Moreover, a beneficial contribution due to the cavities between the nano-sized petals of this structure can also be considered.

The ZnO anodes were tested in a three electrodes cell in the presence of 1 mM NADH (see Figure 3). The current density was calculated by using the ECSA values in order to have normalized values. The CVs of ZnOF and ZnOP samples showed a well-defined oxidation peak at 1.2 V *vs*. Ag/AgCl, that was attributed to NADH oxidation since no peak was observed in absence of NADH. On the contrary, no clear peak was observed when the nanowire morphology was considered. For the studied ZnO-based electrodes, the peak was observed at higher potentials with respect to bare carbon-based electrodes (0.25 V *vs*. Ag/AgCl) [14] or to gold-based anodes (0.69 V *vs*. saturated calomel electrode) reported in literature [32]. For the studied ZnO-based electrodes, the oxidation peak partially overlapped with the increasing of the current because of the water oxidation reaction, which is an application where ZnO has been commonly studied as photocatalyst [50]. By testing the

nanowire structures, no clear peak was observed but only a current increasing due to the water oxidation reaction.

The more promising ZnOF and ZnOP samples were also tested by changing the NADH concentration from 0.1 up to 20 mM. Figure 4 shows a linear relationship between the maximum current density of the peak and the NADH concentration. The slope of the curves is 15 μA·cm$_{\text{ECSA}}^{-2}$·mM^{-1} for ZnOF and 6.6 μA·cm$_{\text{ECSA}}^{-2}$·mM^{-1} for ZnOP. The higher slope was obtained with ZnOF, which indicates that this structure is more sensitive to the NADH concentration.

3.3 Effect of the illumination

The effect of the illumination on the oxidation of NADH was tested only for ZnOP- and ZnOF-based electrodes due to their higher activity. Figure 5 shows the LSV behavior between 0 and 1.6 V *vs*. Ag/AgCl with a chopped illumination condition. This is an easy and quick method to see the photocurrent produced at different applied potentials. It is worth to note that the current density of the oxidation peak of NADH increases with the concentration of NADH, accordingly to the results shown in Figure 3. The highest photocurrent was observed in the absence of NADH (Figure 5, black line), for both ZnOP and ZnOF materials. Considering that the curves are normalized with the calculated ECSA, ZnOP shows a higher photocurrent per square meter than ZnOF. The increase of NADH concentration yielded to a systematic decrease of the photocurrent. This occurs because both NADH and ZnO absorb in the UV region. Thus, the number of photons that reaches the ZnO material is reduced. In fact, with a 20 mM NADH solution (Figure 5, green line), the photocurrent is hardly observed, which means that the illuminated and dark curves are almost the same.

3.4 (Photo)electrochemical oxidation of NADH

The regeneration of NAD$^+$ was tested with the ZnOF- and ZnOP-based electrodes both in dark conditions and under illumination. The tests were carried out in a three electrodes electrochemical cell with an applied potential of 1.2 V vs. Ag/AgCl, which is the same value of the oxidation peak observed for NADH in the CVs (see Figure 3). Figure 6 shows the decrease of NADH concentration in the course of the electrochemical reaction. In dark conditions, the materials show the lowest oxidation rate. The illuminated ZnOF-based electrode shows the highest reaction rate and NADH conversion (58.7%), see Figure 7. A control experiment was conducted by using the bare conductive substrate (FTO), and no oxidation of NADH was observed after 3 h of reaction (data not shown). The higher performance of ZnOF in comparison with ZnOP can be attributed to the higher ECSA of the nanoflower-like film with respect to the porous film, which leads to a higher number of catalytic sites exposed to the electrolyte.

To separate the effect of the illumination from that of the applied potential, an experiment was conducted under illumination and at the OCV, i.e., without applying an external potential. At this condition, a 34% of oxidation of NADH was obtained (see Figure 7). This result reveals that a synergetic effect takes place during the photoelectrochemical oxidation. Thus, the latter is not only the addition of the contribution of the electrochemical regeneration (in dark) and the photochemical regeneration. The sum of the two contributions results in a regeneration of 41.6%, which corresponds to only two third of the value obtained with the photoelectrochemical oxidation at 1.2 V vs. Ag/AgCl (~58.7%).

To determine the stability of the ZnOF-based films, the photoelectrochemical reactions were repeated up to three times with the same film. Generally, the conversion showed a decrease of 3 – 5% after each batch. The differences observed are related to two main reasons:

the photocorrosion of ZnO and the absorption of NAD$^+$ species on the electrode surface during the electrochemical reaction. The photocorrosion issue of ZnO-based electrodes was previously reported for other photocatalytic applications and could be resolved by exploiting a protective shell in the ZnO surface (e.g. of TiO$_2$) [34, 51]. Besides, the physical adsorption of NAD$^+$ is an issue reported for the electrochemical regeneration method [15], and functionalized electrodes with a positive-charged surface were studied to keep NAD$^+$ off of the electrode [52]. The absorption of the coenzyme was confirmed by the FT-IR spectrum of the films after reaction (see SI). The peaks observed at 1068 and 634 cm^{-1}, attributed to phosphate groups, and the peaks at 993 and 936 cm^{-1}, attributed to C-H bonds, indicate the presence of NAD$^+$ on the surface of both the ZnOF- and ZnOP-based films.

3.5 Enzymatic activity of regenerated NAD$^+$

The photoelectrochemical regeneration of NAD$^+$ was confirmed by measuring the activity of the coenzyme in the presence of FDH. The oxidation of formate, catalyzed by FDH (Eq. 2), proceeds only in the presence of NAD$^+$ species in solution. The relative NAD$^+$ activity obtained with the three different studied conditions is reported in Figure 7; a fresh 1 mM solution of NAD$^+$ represents an enzymatic activity of 100%. A control with a fresh 1 mM solution of NADH was used, giving an 8% of relative enzymatic activity. The values of relative activity are similar in number to those of the NADH conversion, thus indicating that most of the oxidized coenzyme was enzymatically active. In the case of photoelectrochemical regeneration at 1.2 V *vs*. Ag/AgCl, the regenerated coenzyme reached an activity of 94%.

14

This result indicates that the structure of the molecule of NAD^+ remains almost intact after the (photo)electrochemical oxidation of NADH and no other modifications took place during the process.

4. Conclusion

NADH was electrochemically oxidized by the ZnO nanostructured electrodes with an anodic peak at 1.2 V *vs*. Ag/AgCl. ZnO demonstrated to be an efficient nanomaterial for the photoelectrochemical regeneration of NAD^+. With the ZnOF-based electrode, an unprecedented regeneration of 58.7% was achieved. The photochemical and electrochemical effects on the oxidation of NADH are not independent from each other but synergistic. The reaction performed with formate dehydrogenase demonstrated that the 94% of the NAD^+ present in the regeneration solution was enzymatically active.

It was also found that smaller concentrations of NADH were needed for the photoelectrochemical regeneration method to reduce the mask effect induced by NADH on the ZnO material. As future improvement, we envision a novel cell configuration where the anode is illuminated at the back could reduce this problem. In addition, the electrochemical cell was not optimized for the process, another configuration could improve the conversion achieved. The cell used has only one compartment for anode and cathode, and platinum wire could reduce the regenerated NAD^+ from the electrolyte solution. Using a two-chamber cell will prevent the reduction of the newly-regenerated NAD^+ and the real reaction rate and conversion could be determined.
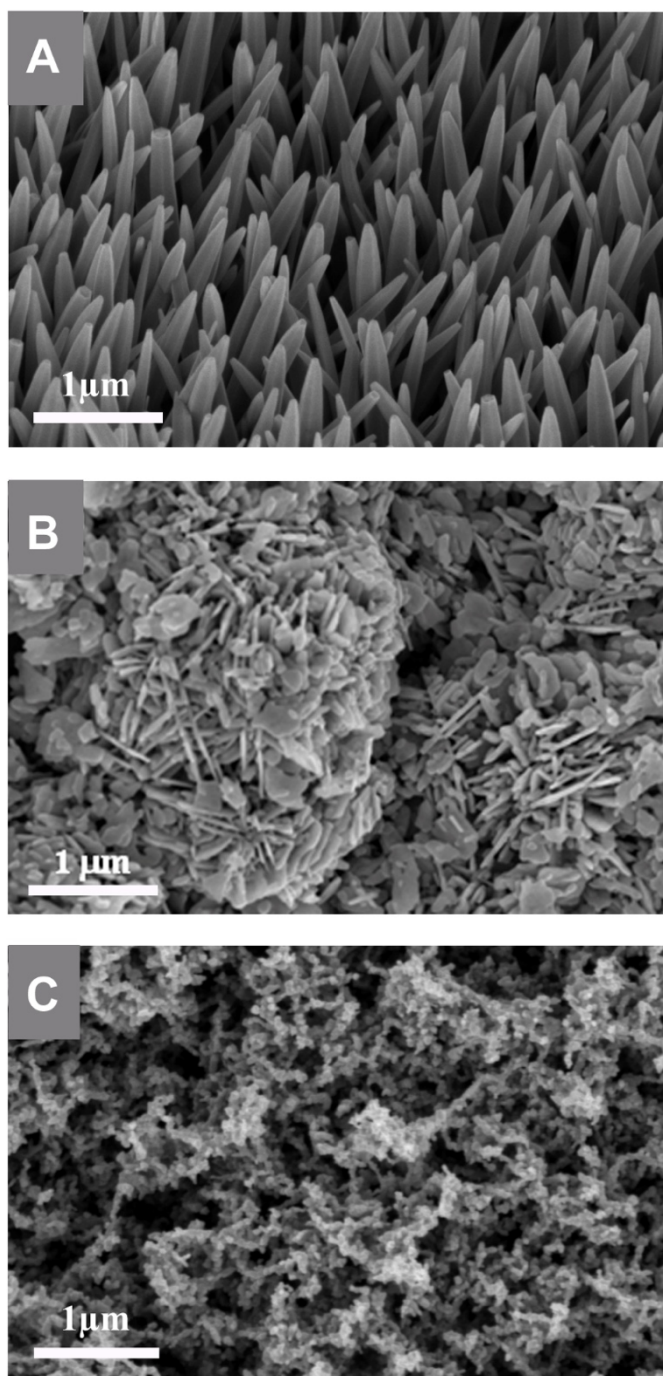
15

FIGURES

Figure 1. FE-SEM images of the synthesized ZnO nanostructures: ZnOW (A), ZnOF (B) and ZnOP (C).
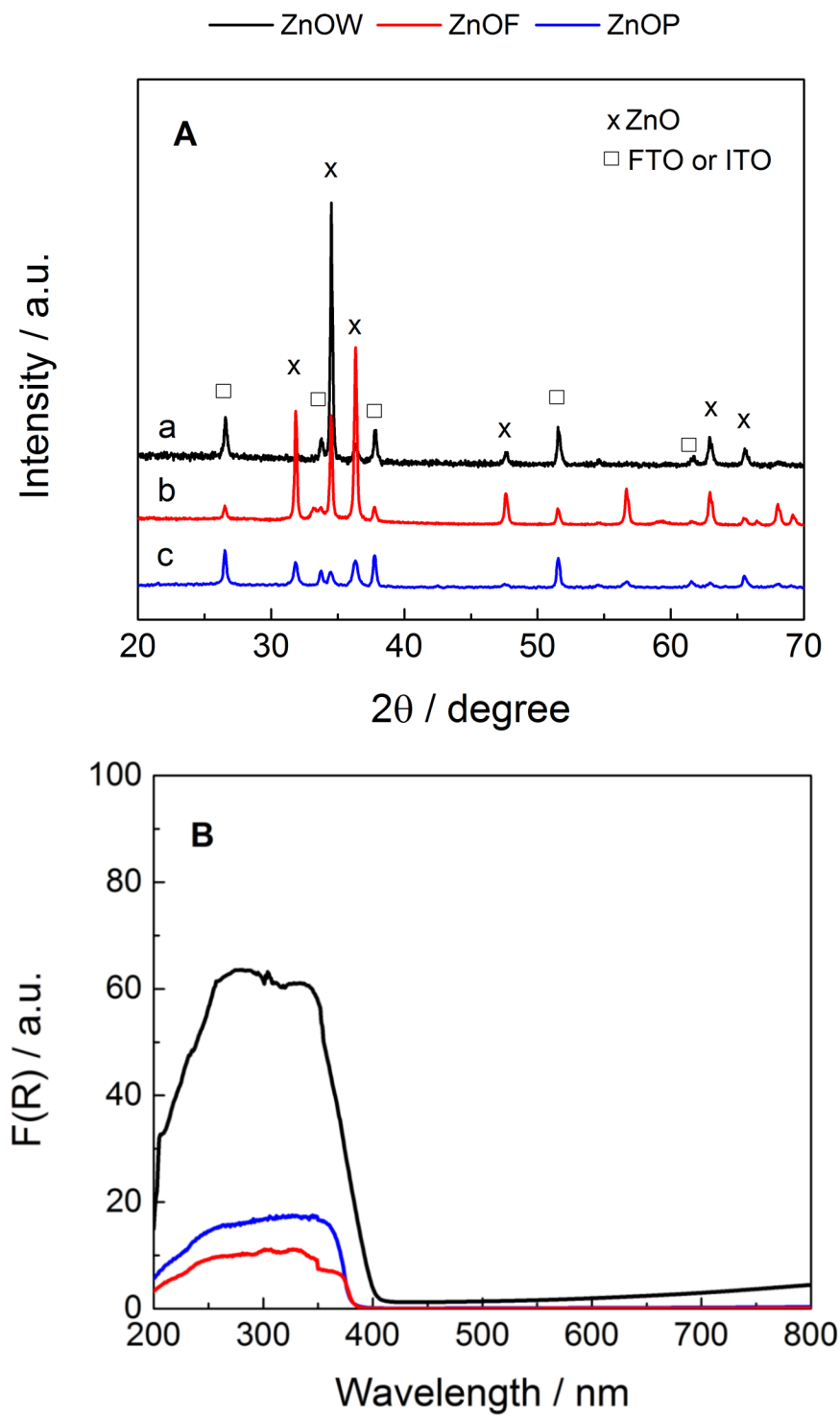
Figure 2. Physicochemical characterization of the different ZnO-based electrodes. A) XRD and B) UV-Vis reflectance F(R) spectra.
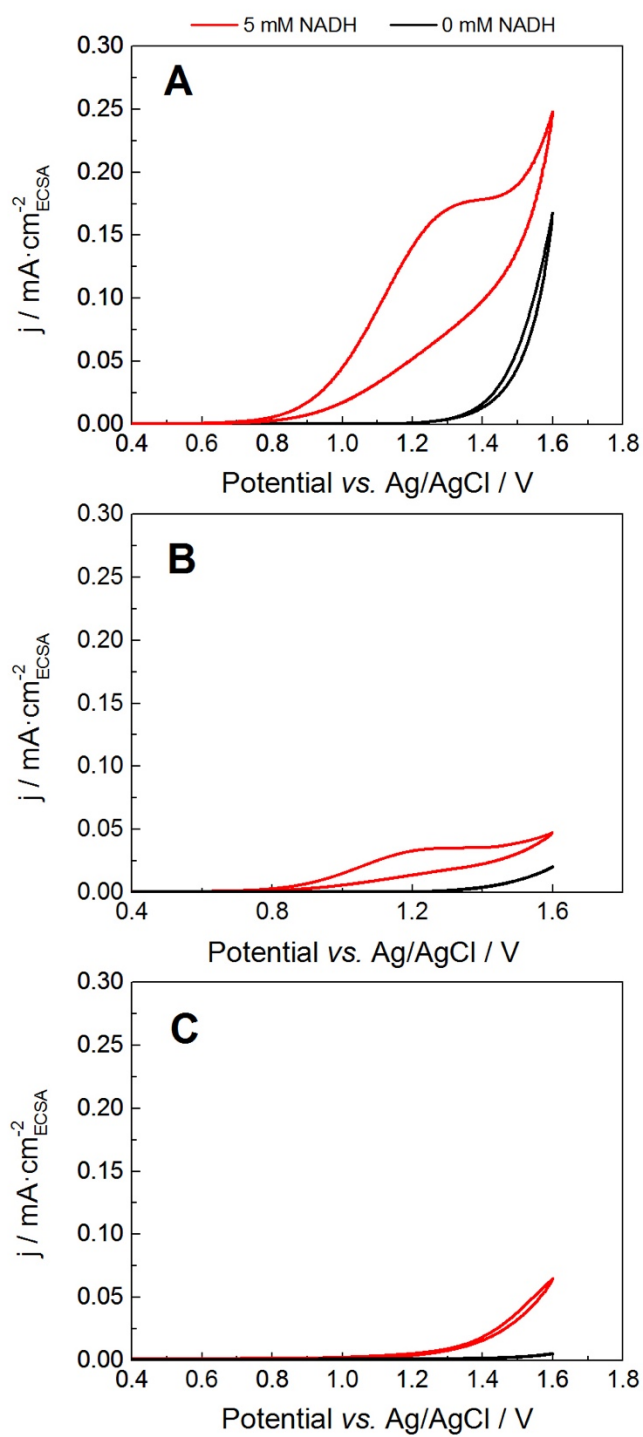
Figure 3. CVs of ZnO films with a solution containing 5 mM NADH (red curves) and in absence of NADH (black curves) for ZnOF (A), ZnOP (B) and ZnOW (C) electrodes.
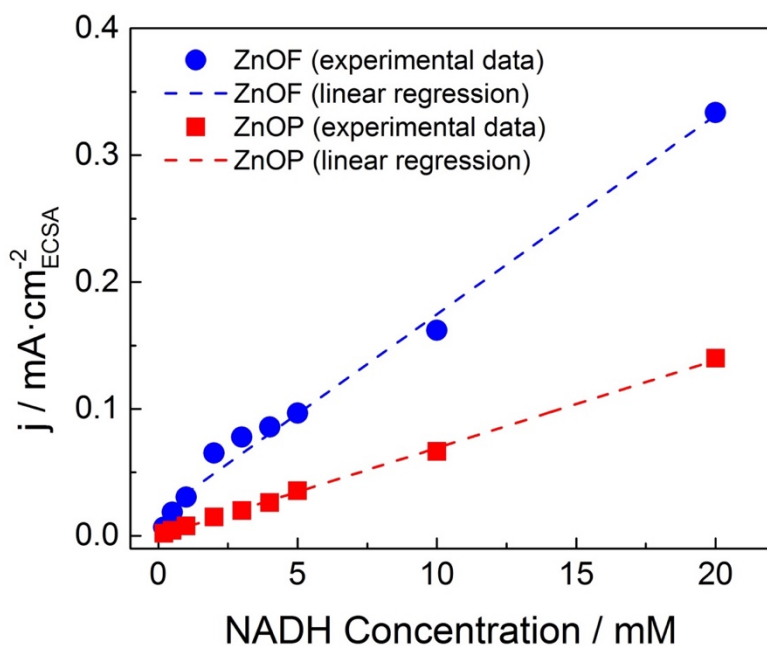
Figure 4. Calibration plot in dark conditions obtained from the anodic peak current of the fourth cycle of the cyclic voltammetry recorded at a scan rate of 20 mV·s^{-1} for ZnO-based electrodes.
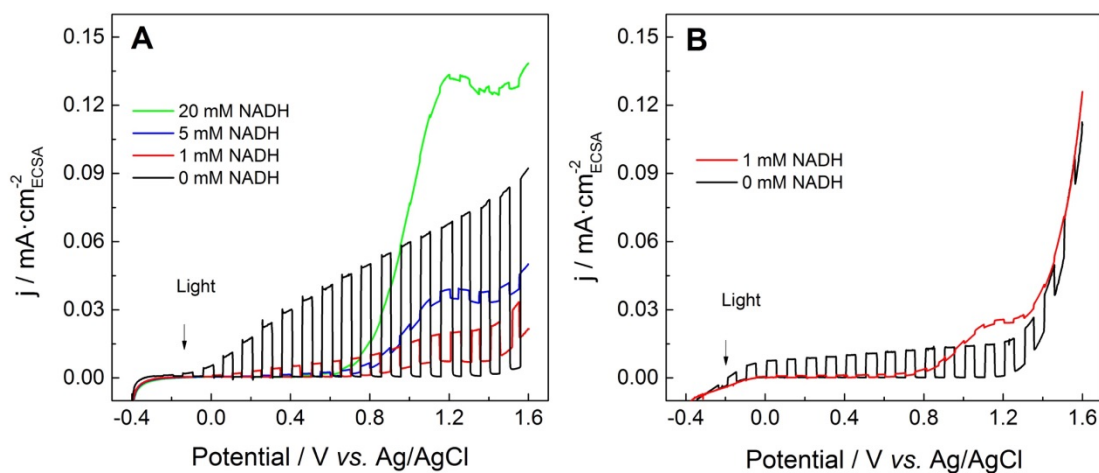

Figure 5. LSV under chopped light and at different NADH concentrations of ZnOP (A) and ZnOF (B) films.
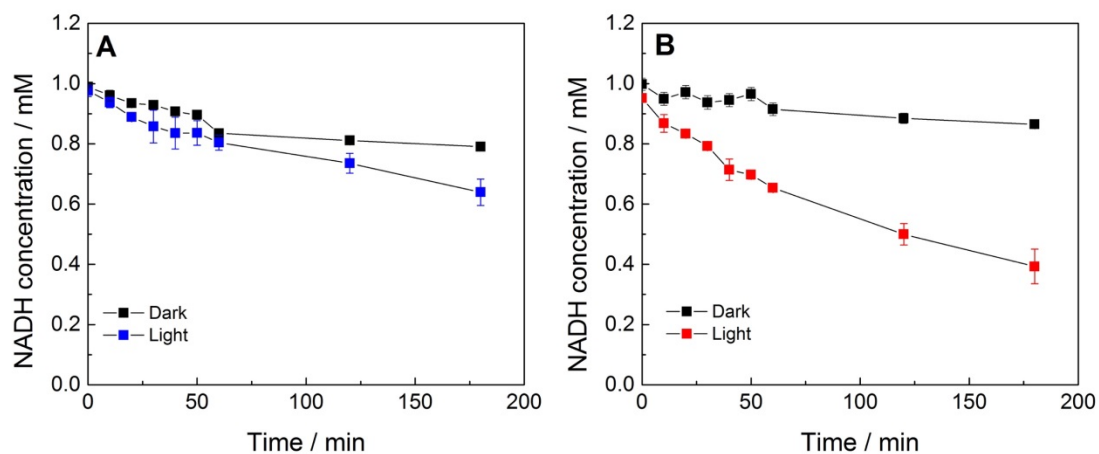
Figure 6. Photoelectrochemical oxidation of NADH with ZnOF (A) and ZnOP (B). In dark condition (circles) or under illumination (squares).
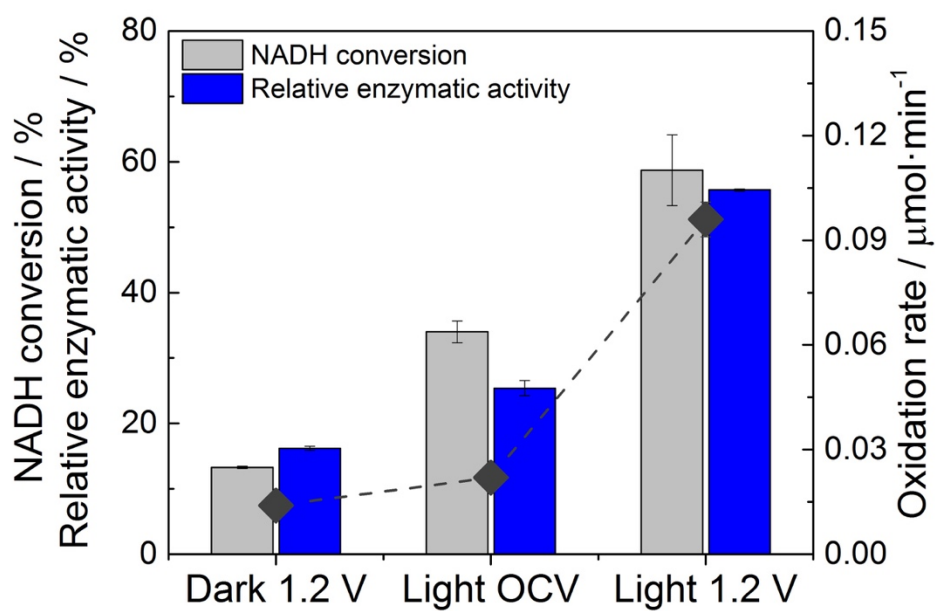

Figure 7. Photoelectrochemical regeneration of NAD^+ with ZnOF electrodes.

TABLES.

Table 1. Specifications of the ZnO films.

Material	GA[a] (cm²)	ECSA[b] (cm²)	Thickness (μm)	E_g (eV)
ZnOW	0.78	0.7978	2.8	3.27
ZnOF	0.78	3.5531	13.3	3.26
ZnOP	0.78	0.7021	1.5	3.29

[a] GA: Geometrical Area, [b] ECSA: Electrochemical surface area

ASSOCIATED CONTENT

Supporting Information. ECSA calculation; Optical characterization of the electrodes.

AUTHOR INFORMATION

Corresponding Author

*(carminna.ottone@pucv.cl)

Present Addresses

Escuela de Ingeniería Bioquímica, Pontificia Universidad Católica de Valparaíso, Av.

Brasil 2085, Valparaiso, Chile

Author Contributions

The manuscript was written through contributions of all authors. All authors have given

approval to the final version of the manuscript.

ABBREVIATIONS

CV, cyclic voltammetry; ECSA, electrochemical surface area; FDH, formate dehydrogenase; FE-SEM, field emission scanning electron microscopy; FTO, fluorine-doped tin oxide; GA, geometrical area; HMT, hexamethylenetetramine; LSV, linear sweep voltammetry; OCV, open circuit voltage; PEC, photoelectrochemical cell; PEI, polyethyleneimine; RF, radio-frequency; UV, ultraviolet; XRD, X-Ray Diffraction.

REFERENCES

1.   Ottone, C.; Bernal, C.; Serna, N.; Illanes, A.; Wilson, L. Enhanced long-chain fatty alcohol oxidation by immobilization of alcohol dehydrogenase from *S. cerevisiae*. *J. Appl. Microbiol.* **2018,** *102*, 237-247.

2.   Ahn, W. S.; Dong, W.; Zhang, Z.; Cantor, J. R.; Sabatini, D. M.; Iliopoulos, O.; Stephanopoulos, G. Glyceraldehyde 3-phosphate dehydrogenase modulates nonoxidative pentose phosphate pathway to provide anabolic precursors in hypoxic tumor cells. *AIChE J* **2018,** *64*, 4289-4296.

3.   Tipton, K. F.; Couée, I. Glutamate dehydrogenase. In *Glutamine and Glutamate Mammals*, CRC Press: **2018**, pp 81-100.

4.   Zheng, Y.-G.; Yin, H.-H.; Yu, D.-F.; Chen, X.; Tang, X.-L.; Zhang, X.-J.; Xue, Y.-P.; Wang, Y.-J.; Liu, Z.-Q. Recent advances in biotechnological applications of alcohol dehydrogenases. *Appl. Microbiol. Biotechnol.* **2017,** *101*, 987-1001.

5.   Barin, R.; Biria, D.; Rashid-Nadimi, S.; Asadollahi, M. A. Enzymatic CO_2 reduction to formate by formate dehydrogenase from *Candida boidinii* coupling with direct electrochemical regeneration of NADH. *J. CO2 Util.* **2018,** *28*, 117-125.

6.   Antiochia, R.; Lavagnini, I.; Pastore, P.; Magno, F. A comparison between the use of a redox mediator in solution and of surface modified electrodes in the electrocatalytic oxidation of nicotinamide adenine dinucleotide. *Bioelectrochemistry* **2004,** *64*, 157-163.

7.   Kochius, S.; Park, J. B.; Ley, C.; Könst, P.; Hollmann, F.; Schrader, J.; Holtmann, D. Electrochemical regeneration of oxidised nicotinamide cofactors in a scalable reactor. *J. Mol. Catal., B Enzym.* **2014,** *103*, 94-99.

8.   Jones, W.; Burnett, J. W. H.; Shi, J.; Howe, R. F.; Wang, X. Improving Photocatalytic Energy Conversion via NAD(P)H. *Joule* **2020,** *4*, 2055-2059.

9.   Liu, W.; Wang, P. Cofactor regeneration for sustainable enzymatic biosynthesis. *Biotechnol. Adv.* **2007,** *25*, 369-384.

10.   Pham, N. H.; Hollmann, F.; Kracher, D.; Preims, M.; Haltrich, D.; Ludwig, R. Engineering an enzymatic regeneration system for NAD(P)H oxidation. *J. Mol. Catal., B Enzym.* **2015,** *120*, 38-46.

11.   Rehn, G.; Pedersen, A. T.; Woodley, J. M. Application of NAD(P)H oxidase for cofactor regeneration in dehydrogenase catalyzed oxidations. *J. Mol. Catal., B Enzym.* **2016,** *134*, 331-339.

12. Hollmann, F.; Hofstetter, K.; Schmid, A. Non-enzymatic regeneration of nicotinamide and flavin cofactors for monooxygenase catalysis. *Trends Biotechnol*. **2006,** *24*, 163-171.

13. Ali, I.; McArthur, M.; Hordy, N.; Coulombe, S.; Omanovic, S. Electrochemical regeneration of the cofactor NADH employing a carbon nanofibers cathode. *Int*. *J*. *Electrochem*. *Sci*. **2012,** *7*, 7675-7683.

14. Munteanu, F.-D.; Mano, N.; Kuhn, A.; Gorton, L. Mediator-modified electrodes for catalytic NADH oxidation: high rate constants at interesting overpotentials. *Bioelectrochemistry* **2002,** *56*, 67-72.

15. Hollmann, F.; Schmid, A. Electrochemical regeneration of oxidoreductases for cell-free biocatalytic redox reactions. *Biocatal*. *Biotransformation* **2004,** *22*, 63-88.

16. Oppelt, K. T.; Gasiorowski, J.; Egbe, D. A. M.; Kollender, J. P.; Himmelsbach, M.; Hassel, A. W.; Sariciftci, N. S.; Knör, G. n. Rhodium-coordinated poly (arylene-ethynylene)-alt-poly (arylene-vinylene) copolymer acting as photocatalyst for visible-light-powered NAD^+/NADH reduction. *J*. *Am*. *Chem*. *Soc*. **2014,** *136*, 12721-12729.

17. Ho, Y.-H.; Periasamy, A. P.; Chen, S.-M. Photoelectrocatalytic regeneration of NADH at poly (4, 4′-diaminodiphenyl sulfone)/nano TiO_2 composite film modified indium tin oxide electrode. *Sens* . *Actuators B Chem*. **2011,** *156*, 84-94.

18. Stufano, P.; Paris, A. R.; Bocarsly, A. Photoelectrochemical NADH Regeneration using Pt-Modified p-GaAs Semiconductor Electrodes. *ChemElectroChem* **2017,** *4*, 1066-1073.

19.   Rocha-Martín, J.; Vega, D.; Bolivar, J. M.; Godoy, C. A.; Hidalgo, A.; Berenguer, J.; Guisán, J. M.; López-Gallego, F. New biotechnological perspectives of a NADH oxidase variant from *Thermus thermophilus* HB27 as NAD$^+$-recycling enzyme. *BMC Biotechnol.* **2011,** *11*, 101.

20.   Ozbakir, H. F.; Garcia, K. E.; Banta, S. Creation of a formate: malate oxidoreductase by fusion of dehydrogenase enzymes with PEGylated cofactor swing arms. *Protein Eng. Des. Sel.* **2018,** *31*, 103-108.

21.   Hirota, R.; Motomura, K.; Kuroda, A. Biological phosphite oxidation and its application to phosphorus recycling. In *Phosphorus Recovery and Recycling*, Springer: **2019**, pp 499-513.

22.   Goswami, P.; Chinnadayyala, S. S. R.; Chakraborty, M.; Kumar, A. K.; Kakoti, A. An overview on alcohol oxidases and their potential applications. *Appl. Microbiol. Biotechnol.* **2013,** *97*, 4259-4275.

23.   Schröder, I.; Steckhan, E.; Liese, A. In situ NAD$^+$ regeneration using 2, 2′-azinobis (3-ethylbenzothiazoline-6-sulfonate) as an electron transfer mediator. *J. Electroanal. Chem.* **2003,** *541*, 109-115.

24.   Tan, B.; Hickey, D. P.; Milton, R. D.; Giroud, F.; Minteer, S. D. Regeneration of the NADH cofactor by a rhodium complex immobilized on multi-walled carbon nanotubes. *Electrochem. Soc..* **2015,** *162*, H102-H107.

25.   Délécouls-Servat, K.; Bergel, A.; Basséguy, R. Surface-modified electrodes for NADH oxidation in oxidoreductase-catalysed synthesis. *J Appl Electrochem*. **2001,** *31*, 1095-1101.

26.   Munteanu, F.-D.; Okamoto, Y.; Gorton, L. Electrochemical and catalytic investigation of carbon paste modified with Toluidine Blue O covalently immobilised on silica gel. *Anal*. *Chim*. *Acta*. **2003,** *476*, 43-54.

27.   Raj, C. R.; Gobi, K. V.; Ohsaka, T. Electrocatalytic oxidation of NADH at the self-assembled monolayer of nickel (II) macrocycle on gold electrode. *Bioelectrochemistry* **2000,** *51*, 181-186.

28.   Manu, B.; Chaudhari, S. Anaerobic decolorisation of simulated textile wastewater containing azo dyes. *Bioresour*. *Technol*. **2002,** *82*, 225-231.

29.   Wu, H.; Tian, C.; Song, X.; Liu, C.; Yang, D.; Jiang, Z. Methods for the regeneration of nicotinamide coenzymes. *Green Chem*. **2013,** *15*, 1773-1789.

30.   Gorton, L.; Domínguez, E. Electrochemistry of NAD(P)$^+$/NAD(P)H. *Encyclopedia of Electrochemistry: Online* **2007**.

31.   Ali, I.; Soomro, B.; Omanovic, S. Electrochemical regeneration of NADH on a glassy carbon electrode surface: The influence of electrolysis potential. *Electrochem*. *Commun*. **2011,** *13*, 562-565.

32.   Rodríguez-Hinestroza, R. A.; López, C.; López-Santín, J.; Kane, C.; Benaiges, M. D.; Tzedakis, T. HLADH-catalyzed synthesis of β-amino acids, assisted by continuous

electrochemical regeneration of NAD$^+$ in a filter press microreactor. *Chem. Eng. Sci.* **2017,** *158*, 196-207.

33. Ottone, C.; Laurenti, M.; Motto, P.; Stassi, S.; Demarchi, D.; Cauda, V. ZnO nanowires: Synthesis approaches and electrical properties. In *Nanowires: Synthesis, Electrical Properties and Uses in Biological Systems*, **2014**, pp 1-57.

34. Hernández, S.; Hidalgo, D.; Sacco, A.; Chiodoni, A.; Lamberti, A.; Cauda, V.; Tresso, E.; Saracco, G. Comparison of photocatalytic and transport properties of TiO$_2$ and ZnO nanostructures for solar-driven water splitting. *Phys. Chem. Chem. Phys.* **2015,** *17*, 7775-7786.

35. Lops, C.; Ancona, A.; Di Cesare, K.; Dumontel, B.; Garino, N.; Canavese, G.; Hérnandez, S.; Cauda, V. Sonophotocatalytic degradation mechanisms of Rhodamine B dye via radicals generation by micro-and nano-particles of ZnO. *Appl. Catal. B* **2019,** *243*, 629-640.

36. Saito, M.; Fujihara, S. Large photocurrent generation in dye-sensitized ZnO solar cells. *Energy Environ. Sci.* **2008,** *1*, 280-283.

37. Laurenti, M.; Cauda, V. ZnO nanostructures for tissue engineering applications. *Nanomaterials* **2017,** *7*.

38. Laurenti, M.; Stassi, S.; Canavese, G.; Cauda, V. Surface Engineering of Nanostructured ZnO Surfaces. *Adv. Mater. Interfaces* **2017,** *4*.

39.   Podrezova, L. V.; Porro, S.; Cauda, V.; Fontana, M.; Cicero, G. Comparison between ZnO nanowires grown by chemical vapor deposition and hydrothermal synthesis. *Appl. Phys. A* **2013,** *113*, 623-632.

40.   Ottone, C.; Bejtka, K.; Chiodoni, A.; Farías, V.; Roppolo, I.; Canavese, G.; Stassi, S.; Cauda, V. Comprehensive study of the templating effect on the ZnO nanostructure formation within porous hard membranes. *New J. Chem.* **2014,** *38*, 2058-2065.

41.   Laurenti, M.; Cauda, V. Porous zinc oxide thin films: Synthesis approaches and applications. *Coatings* **2018,** *8*.

42.   Kumar, S. A.; Chen, S. M. Nanostructured zinc oxide particles in chemically modified electrodes for biosensor applications. *Anal. Lett.* **2008,** *41*, 141-158.

43.   Zhao, Y.; Yan, X.; Kang, Z.; Fang, X.; Zheng, X.; Zhao, L.; Du, H.; Zhang, Y. Zinc oxide nanowires-based electrochemical biosensor for L-lactic acid amperometric detection. *J Nanopart Res.* **2014,** *16*, 2398.

44.   Ali, A.; Ansari, A. A.; Kaushik, A.; Solanki, P. R.; Barik, A.; Pandey, M.; Malhotra, B. Nanostructured zinc oxide film for urea sensor. *Mater. Lett.* **2009,** *63*, 2473-2475.

45.   Tian, K.; Alex, S.; Siegel, G.; Tiwari, A. Enzymatic glucose sensor based on Au nanoparticle and plant-like ZnO film modified electrode. *Mater. Sci. Eng. C.* **2015,** *46*, 548-552.

46.   Rivera, V. F.; Auras, F.; Motto, P.; Stassi, S.; Canavese, G.; Celasco, E.; Bein, T.; Onida, B.; Cauda, V. Length-dependent charge generation from vertical arrays of high-aspect-ratio ZnO nanowires. *Chem. Eur. J.*. **2013,** *19*, 14665-14674.

47.   Laurenti, M.; Canavese, G.; Stassi, S.; Fontana, M.; Castellino, M.; Pirri, C.; Cauda, V. A porous nanobranched structure: An effective way to improve piezoelectricity in sputtered ZnO thin films. *RSC Adv*. **2016,** *6*, 76996-77004.

48.   Pugliese, D.; Bella, F.; Cauda, V.; Lamberti, A.; Sacco, A.; Tresso, E.; Bianco, S. A chemometric approach for the sensitization procedure of ZnO flowerlike microstructures for dye-sensitized solar cells. *ACS Appl*. *Mater*. *Interfaces* **2013,** *5*, 11288-11295.

49.   Cauda, V.; Pugliese, D.; Garino, N.; Sacco, A.; Bianco, S.; Bella, F.; Lamberti, A.; Gerbaldi, C. Multi-functional energy conversion and storage electrodes using flower-like Zinc oxide nanostructures. *Energy* **2014,** *65*, 639-646.

50.   Hamid, S. B. A.; Teh, S. J.; Lai, C. W. Photocatalytic water oxidation on ZnO: a review. *Catalysts* **2017,** *7*, 93.

51.   Hernández, S.; Cauda, V.; Chiodoni, A.; Dallorto, S.; Sacco, A.; Hidalgo, D.; Celasco, E.; Pirri, C. F. Optimization of 1D ZnO@ TiO_2 core–shell nanostructures for enhanced photoelectrochemical water splitting under solar light illumination. *ACS Appl*. *Mater*. *Interfaces* **2014,** *6*, 12153-12167.

52.   Barzegar, A.; Moosavi-Movahedi, A. A.; Ganjali, M. R. Amplification of electrocatalytic oxidation of NADH based on cysteine nanolayers. *J Appl Electrochem*. **2009,** *39*, 1111-1116.